sustainability

MDPI

Article

Adhesive and Cohesive Cracking Analysis of Asphalt Mastics in Contact with Steel Substrates Using an Energy-Based Crack Initiation Criterion

Zhiyang Liu [1,*], Haipeng Wang [2], Jiangcai Chen [3] and Peng Cui [4]

[1] College of Civil and Transportation Engineering, Shenzhen University, Shenzhen 518061, China
[2] Sichuan Highway Planning, Survey, Design and Research Institute Ltd., Chengdu 610041, China
[3] Guangxi Beitou Transportation Maintenance Technology Group Co., Ltd., Nanning 537426, China
[4] Beijing Urban Construction & Development Group Co., Ltd., Bejing 100045, China
* Correspondence: liuzhiyang@szu.edu.cn

Abstract: Adhesive and cohesive properties play a vital role in the durability of asphalt mixtures. As a result of the lack of models characterizing adhesive and cohesive cracking, the occurrence of adhesive and cohesive failure has not been fully formulated by using an explicit mechanical approach. Strain energy density in intact mastics is transformed into adhesive and cohesive surface energies as cracks initiate. This study developed an energy-based crack initiation criterion based on the Griffith model and differentiated adhesive and cohesive cracking. The onset of cracking was identified by the deviation of the measured stress from the linear viscoelastic stress. The released strain energy at the crack initiation balanced the increase in surface energies, thus creating a new adhesive and cohesive surface. Several fracture parameters such as initial crack size, cracking stress, and tensile strength were proposed to analyze the effects of sample thickness, strain rate, temperature, and filler concentration in mastics. Results indicate that the adhesive energy, cohesive energy and strain energy density significantly depend on filler concentration in mastic and test temperature but is independent from sample thickness and strain rate. In particular, the variation of the strain energy density from 20 °C to 35 °C reaches 127.4%, and its decrease is up to 46.9% as the filler concentration in the mastic varies from 0 to 60%. The increase in the sample thickness from 160 μm to 1000 μm results in the 150.0% growth of the initial crack size and 74.4% reduction of the cracking stress. Therefore, increasing the adhesive and cohesive energy can essentially improve the toughness to resist the cracking, and decreasing the mastic thickness enhances the loading capacity. It provides a deep understanding of the mixture cracking from a perspective of adhesive and cohesive surface energies.

Keywords: adhesive and cohesive cracking; crack initiation; energy-based crack initiation; surface energy

check for updates

Citation: Liu, Z.; Wang, H.; Chen, J.; Cui, P. Adhesive and Cohesive Cracking Analysis of Asphalt Mastics in Contact with Steel Substrates Using an Energy-Based Crack Initiation Criterion. *Sustainability* **2023**, *15*, 4415. https://doi.org/10.3390/su15054415

Academic Editor: Syed Minhaj Saleem Kazmi

Received: 25 December 2022
Revised: 24 February 2023
Accepted: 26 February 2023
Published: 1 March 2023

Copyright: © 2023 by the authors. Licensee MDPI, Basel, Switzerland. This article is an open access article distributed under the terms and conditions of the Creative Commons Attribution (CC BY) license (https://creativecommons.org/licenses/by/4.0/).

1. Introduction

Asphalt mixtures are multiphase materials composed of mineral aggregates, bitumen–filler mastic cement, and air voids. Their structural integrity and performance under traffic loading and environment conditions are significantly influenced by the adhesive bond between bitumen and aggregates and by the cohesion of bitumen and/or bitumen–filler mastics [1–5]. The combined action of adhesion loss between bitumen and aggregates and cohesive failure within bitumen–filler mastics can cause mechanical damage, such as cracking and moisture damage. Adhesive failure occurs due to a rupture of the adhesive joint, in which case bitumen adheres to the surface of the aggregate, whereas cohesive failure is considered as the separation of molecules within the interior of the bitumen or mastic [6,7]. The resistance to adhesive and cohesive failure plays a primarily important role in the durability of mixtures.

Research on the adhesive and cohesive failure attract much attention to the mechanism of bitumen–aggregate adhesion and bitumen cohesion. A repeatable, reliable, and practical

method based on a pneumatic adhesion tensile testing instrument has been widely used or modified for bitumen bond strength and uniaxial tensile tests [6–13]. These methods belong to the category of the pull-off tests, in which a sample is under uniaxial tensile stress under a constant loading rate. Numerous researchers utilized the tensile strength and failure type to investigate the effects of diverse factors on the cohesion of the bitumen film and the adhesion of the bitumen–aggregate interface. The chemical composition and the physical and mechanical properties of bitumen and aggregates are widely regarded as crucial factors affecting pull-off strengths and failure types [6,8,9,11–15]. The cohesive strength of mastics was demonstrated to depend on bitumen and its interaction with mineral fillers [16–18]. Moreover, the thin bitumen films were observed to present high pull-off strength. Several testing conditions, such as strain rate, temperature, and moisture, exert a significant impact on adhesion and cohesion [7,14,15,19]. These observations demonstrate that cohesion and adhesion are extremely complicated processes involving not only mechanical behavior but also physicochemical bonding and potential chemical interactions.

The pull-off strength, defined as the maximum tensile stress, is a common parameter used to evaluate cohesion and adhesion [6,20,21]. While the stress reaches the pull-off strength, the mastic cannot resist the loading force due to the coupled effect of crack propagation, nonlinear viscoelasticity, and viscoplasticity in the mastic. As mentioned previously, adhesive and cohesive failure is considered as the rupture of the adhesive joint at the mastic-aggregate interface and the bond of bulk mastic [6]. The adhesive failure is mainly attributed to the large-scale destruction of physicochemical bonding between bitumen polar molecular and active site on the aggregates surface. The cohesive failure of the mastic involves the cracking of the bitumen and the local separation between filler particles and bitumen. It is noted that local adhesive and cohesive cracking occurs in the mastic-aggregate interface and bulk mastic simultaneously [22]. Pull-off strength has a few limitations in mechanically differentiating adhesive and cohesive failure. Isolating crack initiation and propagation from pull-off strength is difficult. The impact of nonlinear viscoelasticity and viscoplasticity at crack initiation is negligible. The mechanical behavior of the mastic at crack initiation could be related to the adhesive and cohesive surface energy by an energy-based crack initiation criterion.

Most previous studies investigated the impacts of diverse factors on tensile strength and introduced fundamental mechanisms, including mechanics and physicochemical bonding, to explain these phenomena [20,21,23]. From the perspective of mechanics, several studies reported fitted relationships between pull-off strength and bitumen stiffness [24,25]. Some researchers developed the correlations of pull-off strength with softening point, penetration, and viscosity [9]. A phenomenological fitting method rather than a rigorous mechanical approach was utilized to characterize the dependence of adhesion and cohesion on the mechanical properties of bitumen. Additionally, physicochemical theory reveals the dominant role of surface free energy in the cohesion of diverse bitumen and the adhesion of bitumen–aggregate combinations [6,13,26]. Short-term and long-term aging significantly change the chemical composition of the bitumen and alter its surface free energy, resulting in the a significantly different wetting and interface adhesion [27]. Nevertheless, the quantitative contribution of surface free energy has not been clearly considered in the measured adhesion and cohesion. Hence, difficulties still arise in developing an analytical approach that incorporates the mechanical behavior of bitumen and surface energy to quantitatively characterize adhesive and cohesive failure.

The present study investigated the adhesive and cohesive cracking of bitumen–filler mastics on stainless steel plates using a uniaxial tensile test with a constant strain rate. The stress and strain in the loading process were monitored to capture the mechanical response of the mastic. An energy-based crack initiation criterion was developed to incorporate the impacts of the mechanical properties and surface free energy on adhesive and cohesive cracking. Tensile tests under different factors, including sample thickness, filler concentration, strain rate, and testing temperature, were performed. The effects of the factors on cracking parameters were systematically analyzed.

2. Development of Energy-Based Crack Initiation Criterion

2.1. Mechanical Response Analysis of Bitumen–Filler Mastic

Mechanical behavior of bitumen–filler mastic under an increasing load is characterized as a stress-strain curve shown in Figure 1. The stress-strain curve of the mastic generally consists of linear viscoelastic, damage accumulation, and failure states. In the linear viscoelastic state, the mastic with intact cohesion in bulk and good adhesion at the mastic–aggregate interface remains its integrity. The mechanical response to the applied load is expressed as a linear viscoelastic formula. While the stress of mastic reaches a critical condition, microcracks arise in bulk and interfacial mastic. The stress of mastic begins to deviate from the linear viscoelastic stress. While neglecting a trace of thermal dissipation under a low-rate loading, the energy derivation from the linear viscoelastic mainly attributes to the surface energy of new microcracks.Accordingly, the crack initiation is identified as the point in a stress-strain curve at which the measured stress begins to deviate from the linear viscoelastic stress. The stress at the crack initiation is the cracking stress σ_0. The increased load continuously provides the released strain energy for the increases in the surface energy of the propagated cracks and plastic deformation, resulting in the progressive deviation from the linear viscoelasticity in the damage accumulation state. The crack growth retards the increase of stress, and the mechanical behavior of mastic eventually enters the failure state beyond the tensile strength σ_f. Therefore, the first step is to model the linear viscoleastic behavior of the mastic under a constant-rate tensile load. Secondly, the cracking initiation is determined by comparing between the linear viscoleastic response and measured stress-strain curve. Subsequently, the adhesive and cohesive surface energies are introduced into the strain energy and then the adhesive and cohesive crack sizes can be obtained.

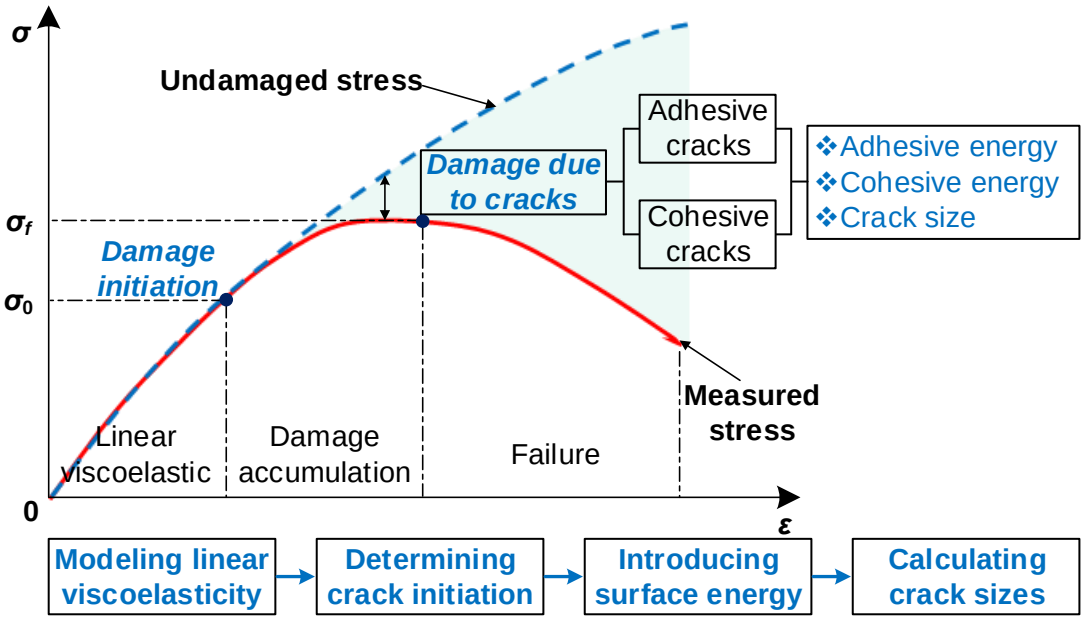

Figure 1. The diagram of tensile failure behavior of bitumen–filler mastic and the route to the development of the energy-based crack criterion.

2.2. Linear Viscoelastic Response

Bitumen–filler mastic in the linear viscoelastic state is a typical viscoelastic material. The mastic is assumed as a continuous and homogenous media with isotropic mechanical properties. Under the assumption of small displacement, the linear viscoelastic response of mastic is formulated by using the generalized Maxwell model. The relaxation modulus E is expressed as

$$E = E_\infty + \sum_{i=1}^{p} E_i e^{-\frac{E_i}{\eta_i}t} \tag{1}$$

where E_∞ and E_i are spring parameters, and η_i is dashpot parameters. P is the number of dashpots. Substituting in the Boltzmann integral [28], the linear viscoelastic stress of mastic under a constant strain rate is given

$$\sigma_{LV}(t) = \int_0^t E(t-\tau)\frac{\partial \varepsilon}{\partial \tau}d\tau = \frac{v}{l_0}\left[E_\infty t + \sum_{i=1}^{p}\eta_i\left(1 - e^{-\frac{E_i}{\eta_i}t}\right)\right] \tag{2}$$

where σ_{LV} is the linear viscoelastic stress; ε and v are the strain and loading displacement rate. L_0 is a material length parameter. Thereby, the strain energy density in linear viscoelastic state ψ_{LV} is obtained by the integral of stress with respect to strain, as shown in Equation (3).

$$\psi_{LV} = \int_0^{\varepsilon(t)} \sigma d\varepsilon = \left(\frac{v}{l_0}\right)^2\left[\frac{1}{2}E_\infty t^2 + \sum_{i=1}^{p}\left(\eta_i t + \frac{\eta_i^2}{E_i}e^{-\frac{E_i}{\eta_i}t} - \frac{\eta_i^2}{E_i}\right)\right] \tag{3}$$

2.3. Crack Initiation Criterion

While a critical condition of micro crack initiation reaches, local adhesive and cohesive cracking occurs, indicative of the appearance of damage and the transition from linear to a nonlinear response. The resistance of the mastic to adhesive and cohesive cracking is characterized by the mechanical parameters at crack initiation. Comparing with the tensile strength or pull-off strength, the parameters at the crack initiation are little affected by the complicated nonlinear viscoelasticity and plastic yielding [17].

Griffith's theory illustrates that the reduction of strain energy balances the increase in the surface energy of the new cracks [29]. The released strain energy of the mastic at crack initiation is converted into the surface energies of new adhesive and cohesive cracks and nonlinear dissipated energy [17]. The nonlinear dissipated energy has been demonstrated to be less than 2.5% of the released energy at the crack initiation. The nonlinear viscoelasticity is considered to be insignificant and negligible at crack initiation. Accordingly, the released strain energy equals the surface energy of new cracks at the crack initiation as shown. The region that releases the strain energy is defined as the energy released zone, as shown in Figure 2. The released strain energy is determined as the product of the strain energy density and the volume of the energy released zone. The increased surface energy is calculated by the surface free energy per area multiplied by the surface area of cracks. The potential energy of the mastic equals the increase in surface energy minus the released energy. The energy release rate, defined as the decrease of the potential energy per unit area of the new crack surface, equals zero at the crack initiation according to Griffith's theory. The crack initiation criterion is expressed as

$$-\frac{d[GA_{s0} - \psi_0 V_{r0}]}{dA_{s0}} = 0 \tag{4}$$

where ψ_0 is the strain energy density at crack initiation, and G is the apparent surface energy per unit area. V_{r0} is the volume of the local energy release zones at crack initiation, and A_{s0} is the surface area of the created crack at crack initiation. The surface area of a new crack is the enclosed area by a circle with a radius of c_0. The energy release zone resembles a solid cone with a base of crack surface, as shown in Figure 2. The height of the energy release zone approximates to πc_0 [29]. An individual initial crack has top and bottom energy released zones and two crack surfaces. The volume of energy release zones and the surface area of new cracks are determined by

$$V_{r0} = 2 \times \frac{1}{3}\pi c_0^2 \times \pi c_0 \tag{5}$$

$$A_{s0} = 2 \times \pi c_0^2 \tag{6}$$

where c_0 is the average initial crack size. Substituting Equations (5) and (6) into Equation (4) and performing differentiation, it yields the relationship between strain energy density and surface free energy expressed as Equation (7).

$$\psi_0 \pi c_0 = 2G \tag{7}$$

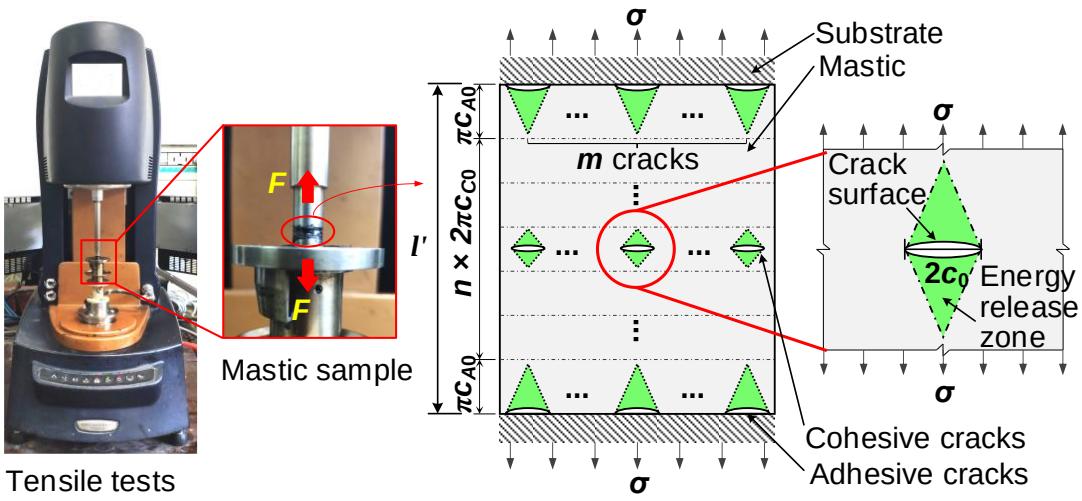

Figure 2. Cohesive and adhesive cracks and energy distribution at crack initiation in a tensile test.

The new cracks consist of adhesive cracks at the interface due to the local mastic–aggregate debonding and cohesive cracks in bulk mastic as a result of the local separation of mastic. The initiation of adhesive and cohesive crack is both dominated by the crack initiation criterion expressed in Equation (7). While neglecting the boundary effects at the interface, the interfacial mastic has an identical energy density to the bulk mastic. Under the assumption of the uniform strain energy density, the crack initiation criterions for adhesive and cohesive cracks are specified as

$$\psi_0 \pi c_{A0} = 2G_A \tag{8}$$

$$\psi_0 \pi c_{C0} = 2G_C \tag{9}$$

where G_A and G_C are the adhesive and cohesive surface energies per unit area. Due to the different adhesive and cohesive surface energies per unit area, the initial adhesive crack size differs from the initial cohesive crack size, which is determined using Equations (8) and (9).

The total surface energy of new cracks is composed of the surface energies of adhesive and cohesive cracks. Since the adhesive cracks arise at the mastic–aggregate interface, the energy release zones of adhesive cracks arise in the vicinity near the top and bottom substrates with a thickness of πc_{A0}. The released strain energy in the energy release zones of adhesive cracks balances the surface energy of new adhesive cracks. Due to the local cohesive failure of mastic, the cohesive cracks appear in the bulk mastic. The released strain energy in the energy release zones of cohesive cracks provides the surface energy of new cohesive cracks. The released strain energy in an energy release zone is only converted into the surface energy of an adjacent adhesive or cohesive crack. In other words, the energy release zones cannot overlap each other. Under the assumption that the potential of local defects existing in the mastic is identical, the probability of the adhesive crack initiation is identical to that of the cohesive crack initiation. If the cylindrical mastic sample is artificially divided into layers along the axis, each mastic layer has the same number of potential cracks due to the identical cracking probability in mastic. The thickness of each layer containing the cohesive cracks in the bulk mastic could be considered as $2\pi c_{C0}$, namely the heights of two energy release zones near the cohesive cracks. Since an adhesive

crack at the interface has an energy release zone, the thickness of layers at the top and bottom interfaces is πc_{A0}, as shown in Figure 2. As a result, the total thickness of the mastic sample is written as

$$l' = \pi c_{A0} + 2\pi c_{C0} \times n + \pi c_{A0} \tag{10}$$

where l' is the mastic thickness. C_{A0} and c_{C0} are the initial adhesive and cohesive crack size. N is the number of cohesive cracking layers. Considering the identical probability of potential cracks in mastic, each layer has m potential cracks. Consequently, the total surface energy equals the sum of surface energies of adhesive and cohesive cracks, as expressed in Equation (11).

$$G \times 2\pi {c_0}^2 \times (n+2)m = G_A \times 2\pi c_{A0}^2 \times 2m + G_C \times 2\pi c_{C0}^2 \times nm \tag{11}$$

where m is the number of potential cracks in each layer. Combining the Equations (7)–(11), it yields

$$n = \frac{\psi_0 l'}{4G_C} - \frac{G_A}{G_C} \tag{12}$$

$$(n+2)G^3 = 2G_A^3 + nG_C^3 \tag{13}$$

$$(n+2)c_0^3 = 2c_{A0}^3 + nc_{C0}^3 \tag{14}$$

The Equation (13) indicates the proportions of adhesive cracking and cohesive cracking in the apparent surface energy. The average initial crack size is related to the surface energies and mastic thickness, as expressed in Equation (14).

3. Materials and Methods

3.1. Materials and Tests

Bitumen–filler mastic is a composite material composed of neat bitumen and mineral filler finer than 75 μm. A neat bitumen with a penetration grade of 60/80 produced by Zhongyou Liaohe Asphalt Ltd. (Panjin, China) was used. The basic properties of bitumen meet the requirements of Technical Specifications of Construction of Highway Asphalt Pavements in China (JTG F40–2004) [30]. Limestone powder finer than 75 μm sieve was selected as the mineral filler. The bitumen and mineral filler were preheated at 155 °C for 4 h and mixed into homogenous mastic by a blender at a speed of 350 r/min within 30 min to avoid marked aging. The hot mastic was poured into a silicone rubber mold and cooled at room temperature to obtain mastic samples with a diameter of 8 mm and an approximate thickness of 2.5 mm. The mastics with six filler volumetric concentrations (0%, 23%, 33%, 40%, 50%, and 60%) were prepared for modulus measurements and tensile failure tests. Original stainless steel plates of discovery hybrid rheometer (DHR) with a diameter of 8 mm were selected. The plate roughness was measured as 0.53 μm ± 0.22 μm by a confocal laser scanning microscope.

3.2. Mechanical Tests

Relaxation modulus of mastics at the temperature of tensile tests was obtained on the basis of modulus master curves within the linear viscoelastic domain. The modulus master curves at a reference temperature were determined by applying the time-temperature superposition principle to the complex moduli at various temperatures and frequencies. The complex moduli were measured by frequency sweep tests under a strain amplitude within the linear viscoelastic domain following the ASTM specification [31]. The temperature and frequency ranges of frequency sweep tests are 10–90 °C and 0.1–30 Hz, respectively. According to the ASTM specification [31], a strain sweep test is utilized to determine the linear viscoelastic limits. The storage modulus of the mastic generally decreases with the increased strain amplitude, and the applied strain at which the storage modulus of mastic is 95 percent of the maximum modulus is defined as the linear viscoelastic limit. The strain range less than the linear viscoelastic limit is the linear viscoelastic domain. The results of strain sweep tests are shown in Figure S3 of Supplementary Material. A

strain amplitude within the overlapped linear viscoelastic domains of various mastics was selected to measure the complex moduli at various frequencies. A detailed procedure of the determination of relaxation modulus from the master curves is elaborated later.

Uniaxial tensile tests of mastics were performed by DHR in a dynamic mechanical analysis mode. Following the specification [31], a mastic sample adhered to preheated plates and reached the required thickness by adjusting the gap between the top and bottom plates. Excess mastic from the periphery was trimmed, as shown in Figure 2 and Figure S1 of Supplementary Material. The mastic was conditioned at the test temperature for at least 30 min to reach the thermal equilibrium. By applying a constant strain rate, the traction and displacement of mastic were recorded automatically during the tensile tests. The traction-displacement curves of the mastics under various factors, including sample thickness (50–200 μm), strain rate (0.01–0.31 s^{-1}), temperature (20–35 °C) and filler volumetric concentration in mastics (0–60%), were investigated. When measuring the mechanical response affected by individual factor, the other factors have to be fixed in the same group of tests. A summary table of uniaxial tensile test configurations under various factors is listed in Table S1 of Supplementary Materials. For instance, in the tests that investigate the effects of the sample's thickness, the other factors such as the composition of the mastic, strain rate and temperature have to be fixed. To ensure the accuracy of test results, the measured traction in tensile tests is expected to be within a moderate range of the DHR maximum limits. Several preliminary tests were conducted to determine the appropriate test configurations. A group of classic failed mastic samples with adhesive and cohesive cracking are shown in Figure S2 of Supplementary Material. More than three replicate samples were measured in subsequent tests.

3.3. Surface Free Energy Tests

Sessile drop method is an accurate, reliable and economical approach for surface free energy measurement of bituminous materials [32]. This approach directly measures the equilibrated contact angles between the mastics and the probe liquids. With the aid of the Yong–Dupre equation, the surface free energy components are calculated from the contact angles. The complete Yong–Dupre equation is expressed as:

$$(1+\cos\theta)\gamma_L = 2\left(\sqrt{\gamma_S^{LW}\gamma_L^{LW}} + \sqrt{\gamma_S^{+}\gamma_L^{-}} + \sqrt{\gamma_S^{-}\gamma_L^{+}}\right) \quad (15)$$

where θ is the contact angle, γ_L is the known surface free energy of probe liquid. γ_S^{LW} and γ_L^{LW} are the Lifshitz–van der Waals components of solid and probe liquids, γ_S^{+} and γ_L^{+} are the Lewis acid components of solid and probe liquids, and γ_S^{-} and γ_L^{-} are the Lewis base components of solid and probe liquids. The determination of three unknown variables in Equation (15) requires the measured contact angles of at least three known probe liquids. Four probe liquids were selected and the surface free energy components were listed in Table S2 of Supplementary Material [33,34] The contact angles of the probe liquids on the mastics were measured using at least five replicate samples.

4. Results and Discussion

4.1. Relaxation Modulus Determination

The relaxation modulus of mastic was determined by a transformation of the modulus master curve. The modulus master curve at a reference temperature was obtained by shifting the modulus at various temperatures and frequencies in accordance with the time-temperature superposition principle. The shift factors at different temperatures were fitted by Williams–Landel–Ferry equations [35]. A typical modulus master curve at 35 °C is shown in Figure S4a of Supplementary Material. The master curve presents a good shifting of modulus curves. The dependence of the mastic's modulus on the temperature and frequency has a similar tendency with the asphalt mixture [17]. Awed used a binomial expression to accurately characterize the shift factors of complex asphalt mixture [17]. However, for the relatively simple asphalt mastic, a linear shift factor expression

is enough competent based on the measured modulus. The master curves at the frequency domain were transformed into relaxation modulus curves at the time domain using TRIOS software [36]. The relaxation modulus curves were fitted using the generalized Maxwell model illustrated as Equation (1). Initial spring and dashpot parameters were assumed to obtain initial relaxation moduli. The relative errors between the predicted and measured modulus were calculated, and the parameters were adjusted to minimize the errors using Solver in Microsoft Excel. A typical relaxation modulus curve is shown in Figure S4b of Supplementary Material. The fitting relaxation modulus curves has a similar shape with the modulus curve of asphalt mixture [17]. Following the above procedure, the spring and dashpot parameters of the bitumen and mastics at 35 °C were obtained and summarized in Table S3 of Supplementary Material. The reference temperatures in master curves and relaxation modulus curves were determined in accordance with the testing temperatures of tensile tests.

4.2. Loading Curves and Crack Initiation Determination

In the linear viscoelastic state, the intact mastic presents linear viscoelastic behavior, and its stress under a constant loading rate is formulated by Equation (2). As the adhesive and cohesive cracks initiate, the measured stress of mastic begins to deviate from the linear viscoelastic stress. The point at which the measured stress begins to deviate from the linear viscoelastic stress identifies the crack initiation. The linear viscoelastic and measured stress curves of mastics were plotted in Figure S5 of Supplementary Material. Inevitable initial stress in tensile tests, $\sigma_{initial}$, is introduced to the linear viscoelastic stress, as shown in Equation (S1) of Supplementary Material. The results suggest the impacts of sample thickness, strain rate, temperature, and filler concentration on the response of mastics. The mastics with various thicknesses have similar linear viscoelastic stress curves. The mastics under various strain rates show different linear viscoelastic stress curves. The linear viscoelastic curve under a higher strain rate has a steeper slope. The mastic at low temperature has high spring parameters but low dashpot parameters, as a result, the mastic at low temperature suggests a steep viscoelastic stress curve. The mastic with a high filler concentration shows a steep linear viscoelastic stress curve. This phenomenon may be attributed to the larger contact surface between filler particle and bitumen in the mastic with a higher filler concentration.

As mentioned previously, the deviation of the measured response from the linear viscoelastic stress results from the initiation and development of the adhesive and cohesive cracks. The point at which the measured stress begins to deviate from the linear viscoelastic stress is the indicator of crack initiation. The thick mastic presents an earlier time of crack initiation and lower cracking stress than the thin mastic. The mastic under a high strain rate begins to crack earlier and has higher cracking stress than that under a low strain rate. The mastic at high temperature suggests premature crack initiation with low cracking stress. A high filler concentration in the mastic delays the crack initiation and increases the cracking stress of the mastic. Besides, more important properties involving the adhesive and cohesive cracking at crack initiation were analyzed later.

4.3. Energy Characteristics and Initial Crack Sizes at Crack Initiation

As the strain energy reaches the critical condition of crack initiation, the released strain energy is converted into the surface energy of new cracks, as formulated by Equation (7). The new cracks consist of adhesive cracks at the mastic–substrate interface and cohesive cracks in the bulk mastic. The surface energies per unit area of the new adhesive and cohesive cracks were measured by using surface free energy measurement and calculated by Equations (16) and (17).

$$G_A = 2\sqrt{\gamma_M^{LW}\gamma_S^{LW}} + 2\sqrt{\gamma_M^{+}\gamma_S^{-}} + 2\sqrt{\gamma_M^{-}\gamma_S^{+}} \tag{16}$$

$$G_C = 2\gamma_M^{LW} + 4\sqrt{\gamma_M^{+}\gamma_M^{-}} \tag{17}$$

where γ_M^{LW} and γ_S^{LW} are the Lifshitz–van der Waals components of the mastic and substrate, γ_M^+ and γ_S^+ are the Lewis acid components of the mastic and substrate, and γ_M^- and γ_S^- are the Lewis base components of the mastic and substrate. The surface free energy components of mastic were measured using a sessile drop method. The surface free energy of stainless steel substrates is cited from the literature [37]. The measured surface free energy components of mastic and adhesive and cohesive surface energies per unit area are listed in Table 1.

Table 1. The surface free energy components of plate and mastic at 25 °C.

Probe Liquids	Filler Content (%)	γ (mJ/m^2)	γ^{LW} (mJ/m^2)	γ^{AB} (mJ/m^2)	γ^+ (mJ/m^2)	γ^- (mJ/m^2)	G_A (mJ/m^2)	G_C (mJ/m^2)
Plate		45.87	40.50	5.37	0.20	36.00		
Mastic	0%	11.49	7.77	3.72	1.28	2.70	50.54	22.98
	23%	13.87	9.49	4.39	1.07	4.48	53.53	27.74
	33%	14.29	10.56	3.72	0.62	5.61	52.91	28.57
	40%	14.58	11.11	3.47	0.49	6.18	53.02	29.16
	50%	14.79	11.95	2.85	0.29	7.05	52.80	29.59

The surface energies of adhesive and cohesive cracks are determined by Equations (12)–(14). As a result of the lack of surface free energy components of known probe liquids at different temperatures in previous literature, the surface free energy components of the mastics and substrate cannot be obtained from the surface free energy tests. The temperature coefficients of the surface free energy of thiophene and stainless steel were used to roughly represent the temperature coefficients of the mastic and substrate, respectively [38,39]. The surface free energy components have similar temperature coefficients [40]. The effects of different factors on the apparent surface energies and strain energy densities at crack initiation are shown in Figure 3. The adhesive and cohesive surface energies per unit area of the mastic remain stable with the increase in thickness and strain rates but decrease with the increased temperatures. The mastics with various filler concentrations have different adhesive and cohesive surface energies due to their different components. The adhesive and cohesive surface energies are the physicochemical properties of the mastic, depending on the temperature and its components but on the geometry and strain rate. Results suggest that the apparent surface energy is roughly independent of the thickness and strain rate but is affected by the test temperature and filler concentration in mastic. The apparent surface energy decreases with the increased temperature except for a slight increase at 35 °C. The phenomenon is related to the initial crack sizes at the crack initiation, which is analyzed later. Regarding the strain energy density at the crack initiation, the mastics under various strain rates have similar strain energy densities. However, the thin mastic has a higher strain energy density than the thick mastic at crack initiation. The strain energy density at crack initiation decreases at high temperature but increases with the filler concentration in mastics.

The initial crack sizes under various factors were plotted in Figure 4. Results suggest that the c_{A0}, c_{C0}, and c_0 increase as the thickness increases. The large cracks in the thick mastic produce a large volume of the energy release zone. For certain surface energy, a large volume of the energy release zone results in a low strain energy density at crack initiation, as expressed as Equation (7). The increased initial crack sizes with the increased thickness explain the decrease in the strain energy density at crack initiation, although the surface energies remain stable for the mastics with various thicknesses, as shown in Figure 3a. The initial crack sizes are observed to be roughly independent of the strain rate, as shown in Figure 4b. The initial crack sizes significantly increase with increased temperature. The increased initial crack sizes decrease the number of cohesive cracking layers, n, as expressed in Equation (10). Since the adhesive surface energy is much larger than the cohesive surface energy, the decreased number of cohesive cracking layers increases the contribution of adhesive surface energy to the apparent surface energy, as shown in Equation (13). It

accounts for the slight increase in the apparent surface energy at 35 °C. The strain energy at the crack initiation is changed into the adhesive and cohesive energies of the new cracks. The rising temperature enhances the molecular thermal motion on the surface and decreases the Gibbs free energy per unit area of both adhesive and cohesive cracks [41,42]. Consequently, the formation of per unit area of new crack surface requires less strain energy at higher temperature, resulting in larger new adhesive and cohesive cracks with a given strain energy. The increase in the initial crack size with the rising temperature can be attributed to the reduction in the adhesive and cohesive surface energies. Moreover, the mastic with a high filler concentration presents small initial crack sizes. It attributes to the strong bitumen–filler interaction due to the increase in the contact surface between bitumen and filler particles. In summary, the mechanical parameters at crack initiation are independent of the strain rate. The geometry of the mastic affects the strain energy density at crack initiation and the initial crack sizes but surface energies. The surface energies of the mastic are sensitive to the temperature and mastic's components due to its physicochemical natural of the mastic.

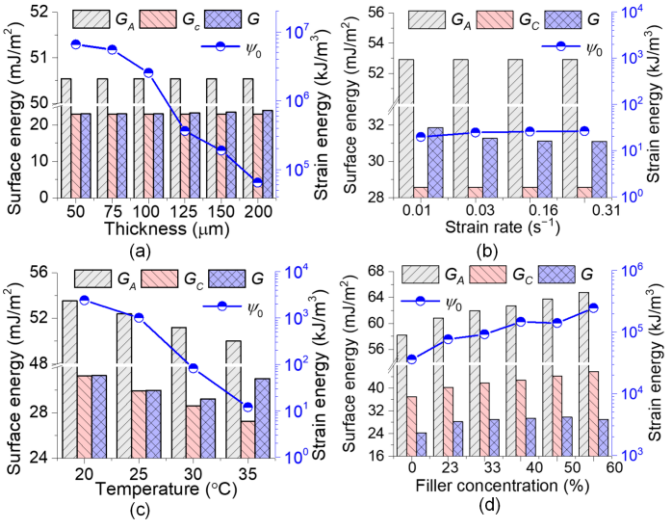

Figure 3. Surface energies and strain energy densities at crack initiation of: (**a**) the bitumen with various thicknesses, (**b**) the mastic under various strain rates, (**c**) the mastic at various temperatures, and (**d**) the mastic with various filler concentrations.

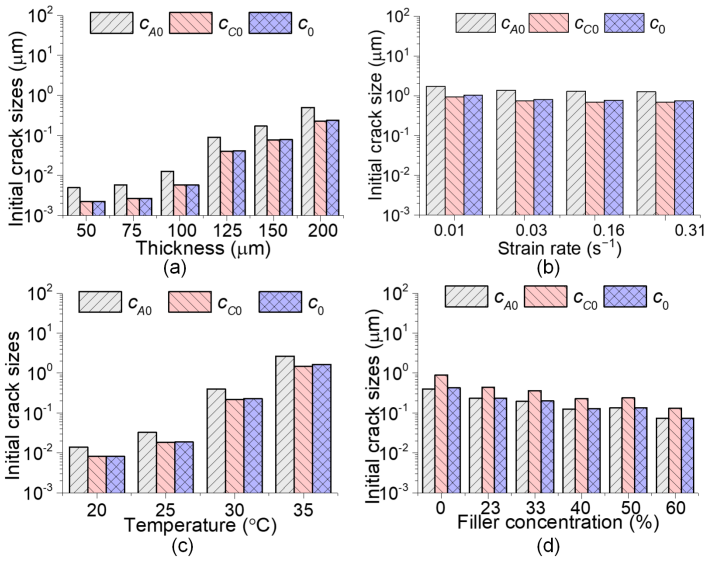

Figure 4. Initial crack sizes of: (**a**) the bitumen with various thicknesses, (**b**) the mastic under various strain rates, (**c**) the mastic at various temperatures, and (**d**) the mastic with various filler concentrations.

4.4. Cracking Stress and Tensile Strength

Cracking stress is the stress that the mastic endures at the crack initiation. Tensile strength is the maximum stress of the mastic during the whole loading process. In comparison, the crack stress has an explicit mechanical conception that is an indication of the onset of a fracture process; whereas the tensile strength results from the complex damage mechanisms including the crack destabilization, nonlinear viscoelasticity, and plasticity. The cracking stress has the advantage to characterize crack initiation. The cracking stresses and tensile strengths of mastics under different factors were depicted in Figure 5. Results show that the cracking stress and tensile strength have a similar trend under various factors. Figure 5a,b suggest that the cracking stress and the tensile strength decrease with the increased thickness but increase under a high strain rate. The thick mastic with more bulk mastic inextricably introduces more potential defects and provides conditions to large initial crack sizes. The increased initial crack size decreases the strain energy density and cracking stress at crack initiation. The time-dependent viscoelasticity of mastic is responsible for the increase of cracking stress and tensile strength under a high strain rate. The mastic does not respond immediately and presents high modulus under a high strain rate. Figure 5c,d suggest that the cracking stress and tensile strength of mastic markedly decrease with the rising temperature but increases with the increased filler volumetric concentration in mastic. The high temperature weakens the cross-linked colloidal structure of bitumen and decreases the stress-resistance of the mastic. Lower surface energy requirement at a higher temperature, as shown in Figure 3c, aggravates the crack initiation at a low stress, resulting in a decreased cracking stress with the rising temperature. Weak cross-link structure of mastic at a high temperature has a weak resistance to the stretching and sliding of molecular chains under the stress, leading to a low tensile strength at the high temperature. Moreover, the high filler concentration in the mastic increases the surface of the filler particle. Considerable free bitumen is adsorbed on the filler particle and converts into the adsorbed bitumen. The polar bitumen molecules could orderly oriented under the intermolecular interaction of the active site on the mineral surface, and it leads to a high modulus and adhesion of the adsorbed bitumen [43,44]. The adsorbed bitumen has stable structure and high resistance to the external stress, leading to the significant increase of the cracking stress and tensile strength. Without prejudice to other performance, proper increase in the filler concentration of the mastic benefit the improvement of the cracking resistance and loading capacity.

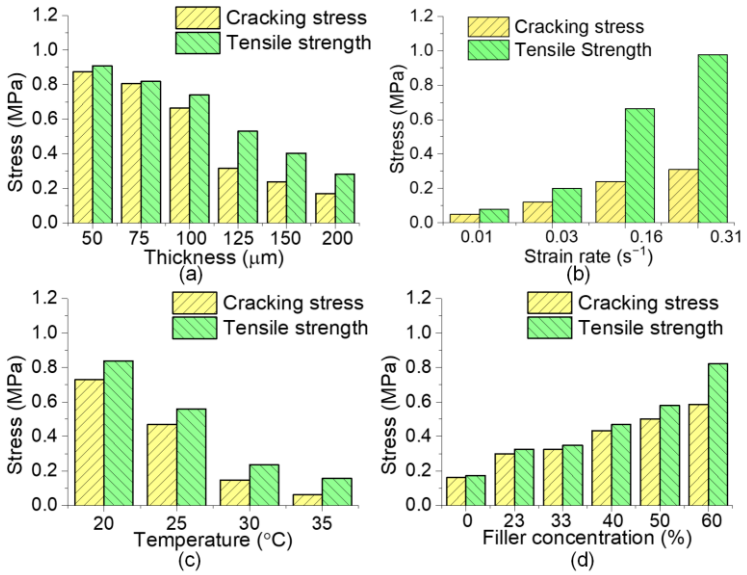

Figure 5. Cracking stresses and tensile strengths of: (**a**) the bitumen with various thicknesses, (**b**) the mastic under various strain rates, (**c**) the mastic at various temperatures, and (**d**) the mastic with various filler concentrations.

The cracking stress and tensile strength may be related to the average initial crack sizes. The crack stress ratios and tensile strength ratios of different mastics under diverse factors are shown in Figure S6 of Supplementary Materials. Results suggest an inverse linear correlation between the cracking stress or tensile strength and the average initial crack size at double logarithm coordinates. The curves are well fitted by power functions with negative exponents, indicative of an adverse impact of average initial crack size on the crack initiation.

5. Conclusions and Summaries

Even though the uniaxial tensile test is widely employed to investigate adhesive and cohesive failures of asphaltic materials, rare quantitative characterization of the crack initiation has been explicitly and mechanically related to the adhesive and cohesive energies on the basis of fracture mechanics. This study developed an energy-based crack initiation criterion to determine the conversion of the strain energy into the adhesive and cohesive energies. Several key parameters such as initial crack sizes, and cracking stress at the crack initiation were proposed to analyze the adhesive and cohesive cracking of the mastics.

The variation of filler concentration in the mastic changes the composition of mastic, resulting in different mechanical and physicochemical properties. The temperature significantly affects the cohesive and adhesive surface energy. Therefore, the filler concentration and temperature exhibit notable influence on the initial crack size and cracking stress. However, the sample thickness could hardly influence the adhesive and cohesive energies but can change the cracking stress and initial crack size. The strain rate can only affect the cracking size. It indicates that the required energy for crack initiation is only related to the physicochemical natures of the mastic and substrates but independent from the mechanical condition. Therefore, increasing the cohesive and adhesive energies of the mastic can essentially enhance the toughness that resists the cracking. Even though the mastic thickness has limited action to the toughness, its significant effect on the cracking stress implies the feasibility of the improvement of loading resistance through decreasing the mastic thickness. It provides a deep insight into the cohesive and adhesive failure from a perspective of energy conservation and promotes the accurate prediction of the fracture behavior of asphalt mixture.

The energy-based crack initiation criterion is developed based on the viscoelastic theory of the asphaltic materials with the assumption that the dissipated strain energy is considered to balance the adhesive and cohesive energies. Consequently, this model is feasible for the cracking of asphaltic materials at a low and moderate temperature. The crack initiation model considering other dissipated energy will be study in the future.

Supplementary Materials: The following supporting information can be downloaded at: https://www.mdpi.com/article/10.3390/su15054415/s1. The supplementary material includes five sections: Section S1 is the uniaxial tensile tests of mastic under various factors, Section S2 is the surface free energy components of probe liquids in surface energy tests, Section S3 is the demonstration of relaxation modulus calculation, Section S4 is the measured stress and linear viscoelastic stress curves for different mastics, and Section S5 is the correlation of the crack stress and tensile strength with the initial crack size. It is available free of charge on the website.

Author Contributions: Conceptualization, Z.L.; Formal analysis, Z.L.; Investigation, P.C.; Writing—original draft, Z.L.; Writing – review & editing, H.W.; Visualization, J.C.; Project administration, P.C. All authors have read and agreed to the published version of the manuscript.

Funding: This work was supported by the National Natural Science Foundation of China [grant numbers 52108410], and China Postdoctoral Science Foundation [grant numbers 2022T150432, 2021M702260], and Sichuan Transportation Science and Technology Project [grant numbers 2021-A-14].

Data Availability Statement: Data is contained within the article and Supplementary Materials.

Conflicts of Interest: The authors declare no conflict of interest.

References

1. Poulikakos, L.D.; Tiwari, M.K.; Partl, M.N. Analysis of Failure Mechanism of Bitumen Films. *Fuel* **2013**, *106*, 437–447. [CrossRef]
2. Mo, L.T.; Huurman, M.; Woldekidan, M.F.; Wu, S.P.; Molenaar, A.A.A. Investigation into Material Optimization and Development for Improved Ravelling Resistant Porous Asphalt Concrete. *Mater. Des.* **2010**, *31*, 3194–3206. [CrossRef]
3. Airey, G.D.; Collop, A.C.; Zoorob, S.E.; Elliott, R.C. The Influence of Aggregate, Filler and Bitumen on Asphalt Mixture Moisture Damage. *Constr. Build. Mater.* **2008**, *22*, 2015–2024. [CrossRef]
4. Cebon, D. Interaction between Heavy Vehicles and Roads. *SAE Tech. Pap. Ser.* **2010**, *1*, 23–38. [CrossRef]
5. Azam, A.M.; El-Badawy, S.M.; Alabasse, R.M. Evaluation of Asphalt Mixtures Modified with Polymer and Wax. *Innov. Infrastruct. Solut.* **2019**, *4*, 43. [CrossRef]
6. Moraes, R.; Velasquez, R.; Bahia, H.U. Measuring the Effect of Moisture on Asphalt-Aggregate Bond with the Bitumen Bond Strength Test. *Transp. Res. Rec. J. Transp. Res. Board* **2011**, *2209*, 70–81. [CrossRef]
7. Chaturabong, P.; Bahia, H.U. Effect of Moisture on the Cohesion of Asphalt Mastics and Bonding with Surface of Aggregates. *Road Mater. Pavement Des.* **2018**, *19*, 741–753. [CrossRef]
8. Canestrari, F.; Cardone, F.; Graziani, A.; Santagata, F.A.; Bahia, H.U. Adhesive and Cohesive Properties of Asphalt-Aggregate Systems Subjected to Moisture Damage. *Road Mater. Pavement Des.* **2010**, *11*, 11–32. [CrossRef]
9. Omar, H.A.; Yusoff, N.I.M.; Ceylan, H.; Sajuri, Z.; Jakarni, F.M.; Ismail, A. Investigation of the Relationship between Fluidity and Adhesion Strength of Unmodified and Modified Bitumens Using the Pull-off Test Method. *Construction and Building Materials* **2016**, *122*, 140–148. [CrossRef]
10. Copeland, A. *Influence of Moisture on Bond Strength of Asphalt-Aggregate Systems*; Cambridge University Press: Cambridge, UK, 2007.
11. Bahia, H.; Moraes, R.; Velásquez, R. Measuring Asphalt-Aggregate Bond Strength under Different Conditions. In Proceedings of the 2nd International Conference on Transport Infrastructures (ICTI), São Paulo, Brazil, 4–6 August 2010.
12. Xie, J.; Chen, Z.; Pang, L.; Wu, S. Implementation of Modified Pull-off Test by UTM to Investigate Bonding Characteristics of Bitumen and Basic Oxygen Furnace Slag (BOF). *Constr. Build. Mater.* **2014**, *57*, 61–68. [CrossRef]
13. Zhang, J.; Apeagyei, A.K.; Airey, G.D.; Grenfell, J.R.A. Influence of Aggregate Mineralogical Composition on Water Resistance of Aggregate-Bitumen Adhesion. *Int. J. Adhes. Adhes.* **2015**, *62*, 45–54. [CrossRef]
14. Wang, D.; Yi, J.; Feng, D. Modelling and Laboratory Studies on the Adhesion Fatigue Performance for Thin-Film Asphalt and Aggregate System. *Sci. World J.* **2014**, *2014*, 819083. [CrossRef] [PubMed]
15. Zhang, J.; Airey, G.D.; Grenfell, J.R.A. Experimental Evaluation of Cohesive and Adhesive Bond Strength and Fracture Energy of Bitumen-Aggregate Systems. *Mater. Struct. /Mater. Constr.* **2016**, *49*, 2653–2667. [CrossRef]
16. Kim, Y.-R.; Little, D.N.; Lytton, R.L. Fatigue and Healing Characterization of Asphalt Mixtures. *J. Mater. Civ. Eng.* **2003**, *15*, 75–83. [CrossRef]
17. Awed, A.M.; Tarbay, E.W.; El-Badawy, S.M.; Azam, A.M. Performance Characteristics of Asphalt Mixtures with Industrial Waste/by-Product Materials as Mineral Fillers under Static and Cyclic Loading. *Road Mater. Pavement Des.* **2022**, *23*, 335–357. [CrossRef]
18. Tarbay, E.W.; Azam, A.M.; El-Badawy, S.M. Waste Materials and By-Products as Mineral Fillers in Asphalt Mixtures. *Innov. Infrastruct. Solut.* **2018**, *4*, 5. [CrossRef]
19. Xu, M.; Yi, J.; Feng, D.; Huang, Y.; Wang, D. Analysis of Adhesive Characteristics of Asphalt Based on Atomic Force Microscopy and Molecular Dynamics Simulation. *ACS Appl. Mater. Interfaces* **2016**, *8*, 12393–12403. [CrossRef]
20. Filonzi, A.; Komaragiri, S.; Hajj, R.; Trevino, M.; Hazlett, D.; Mahmoud, E.; Bhasin, A. A Method to Evaluate the Tensile Strength and Ductility of Asphalt Binders Using a Thin Confined Film. *Int. J. Pavement Eng.* **2022**, 1–12. [CrossRef]
21. Hajj, R.; Hure, R.; Bhasin, A. Evaluation of Stiffness, Strength, and Ductility of Asphalt Binders at an Intermediate Temperature. *Transp. Res. Rec.* **2017**, *2632*, 44–51. [CrossRef]
22. Luo, X.; Ph, D.; Luo, R.; Ph, D.; Asce, M.; Lytton, R.L.; Ph, D.; Asce, F. Energy-Based Crack Initiation Criterion for Viscoelastoplastic Materials with Distributed Cracks. *J. Eng. Mech.* **2015**, *141*, 1–14. [CrossRef]
23. Bhasin, A.; Little, D.N.; Vasconcelos, K.L.; Masad, E. Surface Free Energy to Identify Moisture Sensitivity of Materials for Asphalt Mixes. *Transp. Res. Rec.* **2007**, *2001*, 37–45. [CrossRef]
24. Huang, W.; Lv, Q. Investigation of Critical Factors Determining the Accuracy of Binder Bond Strength Test to Evaluate Adhesion Properties of Asphalt Binders. *J. Test. Eval.* **2016**, *45*, 20150444. [CrossRef]
25. Bitumen Testing-an Introduction to the Use of Test Methods at the Koninklijke/Shell Laboratorium, Amsterdam. Available online: https://trid.trb.org/view/1177740 (accessed on 25 February 2023).
26. Bhasin, A. Development of Methods to Quantify Bitumen-Aggregate Adhesion and Loss of Adhesion Due to Water. Ph.D. Dissertation, Texas A&M University, College Station, TX, USA, 2007.
27. Xiao, R.; Huang, B. Moisture Damage Mechanism and Thermodynamic Properties of Hot-Mix Asphalt under Aging Conditions. *ACS Sustain. Chem. Eng.* **2022**, *10*, 14865–14887. [CrossRef]
28. Allen, D.H.; Searcy, C.R. A Micromechanical Model for a Viscoelastic Cohesive Zone. *Int. J. Fract.* **2001**, *107*, 159–176. [CrossRef]
29. Gdoutos, E.E. *Fracture Mechanics: An Introduction*; Solid Mechanics and Its Applications; Springer: Dordrecht, The Netherlands, 2005; ISBN 978-1-4020-2863-2.

30. MTPRC. *Technical Specifications for Construction of Highway Asphalt Pavements (JTG F40-2004)*; China Communications Press: Beijing, China, 2004.
31. *ASTM D7175-15*; Standard Test Method for Determining the Rheological Properties of Asphalt Binder Using a Dynamic Shear Rheometer. ASTM International: West Conshohocken, PA, USA, 2012.
32. Koc, M.; Bulut, R. Assessment of a Sessile Drop Device and a New Testing Approach Measuring Contact Angles on Aggregates and Asphalt Binders. *J. Ofmaterials Civ. Eng.* **2014**, *26*, 391–398. [CrossRef]
33. Van Oss, C.J. *Interfacial Forces in Aqueous Media*; CRC Press: New York, NY, USA, 2006.
34. Dann, J.R. Forces Involved in the Adhesive Process Ih Nondispersion Forces at Solid-Liquid Interfaces. *J. Colloid Interface Sci.* **1970**, *32*, 321–331. [CrossRef]
35. Williams, M.L.; Landel, R.F.; Ferry, J.D. The Temperature Dependence of Relaxation Mechanisms in Amorphous Polymers and Other Glass-Forming Liquids. *J. Am. Chem. Soc.* **1955**, *77*, 3701–3707. [CrossRef]
36. Ferry, J.D. *Viscoelastic Properties of Polymers*; John Wiley & Sons: New York, NY, USA, 1980.
37. Clint, J.H.; Wicks, A.C. Adhesion under Water: Surface Energy Considerations. *Int. J. Adhes. Adhes.* **2001**, *21*, 267–273. [CrossRef]
38. Jasper, J.J.; Jasper, J.J. The Surface Tension of Pure Liquid Compounds. *J. Phys. Chem. Ref. Data* **1972**, *841*, 841–1010. [CrossRef]
39. Effect of Temperature on the Surface Energy of Solids. Available online: https://warwick.ac.uk/fac/cross_fac/sciencecity/programmes/internal/themes/am2/booking/dropshapeanalyser/effect_of_temperature_on_the_surface_energy_of_solids.pdf (accessed on 25 February 2023).
40. Little, D.N.; Bhasin, A. *Using Surface Energy Measurements to Select Materials for Asphalt Pavement*; Transportation Research Board: Washington, DC, USA, 2006; ISBN 978-0-309-43174-3.
41. Xing, M.; Pathak, A.-D.; Sanyal, S.; Peng, Q.; Liu, X.; Wen, X. Temperature-Dependent Surface Free Energy and the Wulff Shape of Iron and Iron Carbide Nanoparticles: A Molecular Dynamics Study. *Appl. Surf. Sci.* **2020**, *509*, 144859. [CrossRef]
42. Baidakov, V.G.; Protsenko, S.P.; Tipeev, A.O. Temperature Dependence of the Crystal-Liquid Interfacial Free Energy and the Endpoint of the Melting Line. *J. Chem. Phys.* **2013**, *139*, 224703. [CrossRef]
43. Chen, J.-S.; Peng, C.-H. Analyses of Tensile Failure Properties of Asphalt-Mineral Filler Mastics. *J. Mater. Civ. Eng.* **2002**, *10*, 256–262. [CrossRef]
44. Dong, Z.; Liu, Z.; Yang, C.; Gong, X. Viscosity Characterization of Confined Bitumen Considering Microaggregate-bitumen Interactions. *Comput.-Aided Civ. Infrastruct. Eng.* **2020**, *35*, 1261–1275. [CrossRef]

Disclaimer/Publisher's Note: The statements, opinions and data contained in all publications are solely those of the individual author(s) and contributor(s) and not of MDPI and/or the editor(s). MDPI and/or the editor(s) disclaim responsibility for any injury to people or property resulting from any ideas, methods, instructions or products referred to in the content.